INTERNATIONAL JOURNAL FOR NUMERICAL METHODS IN FLUIDS, VOL. 14, 1437–1452 (1992)

AN INVISCID/VISCOUS COUPLING APPROACH FOR VORTEX FLOW FIELD CALCULATIONS

K. D. LEE AND S. A. BRANDT

Department of Aeronautical and Astronautical Engineering, 104 Transportation Building, University of Illinois, Urbana, IL 61801, U.S.A.

SUMMARY

A new computational approach is developed for the analysis of vortex-dominated flow fields around highly swept wings at high angles of attack. In this approach an inviscid Euler technology is coupled with viscous models, similar to inviscid/boundary layer coupling. The viscous nature of the vortex core is represented by an algebraic model derived from the Navier–Stokes equations. The approach also accounts for the effects of the viscous shear layer near a wing surface through a modified surface boundary condition. The inviscid/viscous coupling consistently provides improved predictions of leading edge separation, vortex bursting and secondary vortex formation at relatively low computational cost. Results for several cases are compared with wind tunnel tests and other Euler and Navier–Stokes solutions

KEY WORDS Vortex flow aerodynamics High angle of attack Delta wing Viscous vortex models Vortex separation and bursting Computational fluid dynamics

1. INTRODUCTION

Flow fields involving leading edge vortex separation are strongly non-linear and viscous. Air viscosity plays a dominant role in producing the leading edge vortex separation and vortex bursting for highly swept wings at high angles of attack. In addition, the overall flow field structure is very sensitive to the presence of the vortex system. Therefore the flow model should include viscous terms to represent the complex flow structure. The use of the Navier–Stokes equations requires that the grid size be compatible with the characteristic length scale of air viscosity. This leads to large memory and computer time requirements, especially for high-Reynolds-number flows, making the solution process expensive. Furthermore, the resulting solutions are contaminated by numerical viscosity which is introduced through finite truncations and the grid systems used. In some cases the numerical viscosity may have a greater effect on the solutions than the physical viscosity terms. The Navier–Stokes formulation is also hampered by the lack of an adequate turbulence model.

Euler solutions are usually less expensive than Navier–Stokes solutions because viscosity effects are not included. This cost advantage is partly due to the use of simpler equations but primarily due to the use of coarser grids than those used by Navier–Stokes solvers. Although the Euler formulation can give adequate representation of most portions of the flow field, it often fails to resolve the details of vortex dynamics. Numerical viscosity in Euler codes can trigger such viscous effects as leading edge separation and vortex bursting if defined in the same direction as the physical viscosity. However, the viscous physics cannot be quantitatively represented. Although Euler solutions can produce a flow structure similar to that of the actual physics, many

0271–2091/92/121437–16$08.00
© 1992 by John Wiley & Sons, Ltd.
Received May 1991
Revised November 1991

important flow features cannot be captured at the correct flow conditions with the Euler formulation. Better models describing the vortical flows are needed to represent the viscous physics and to minimize the numerical contaminations.

Many computational efforts have been made to predict steady vortex-dominated flow fields based on the Euler and Navier–Stokes equations.[1-6] Available simulation technologies and physical aspects were reviewed by several authors.[7,8] Some investigators were able to simulate vortex breakdown and generate secondary vortices.[9,10] Effects of grid topology and grid density on the resulting flow solutions were also studied.[10-12] While significant progress has been made, present technologies still have many limitations for understanding vortices and practical applications.

This paper describes a method which uses the Euler formulation but includes viscous physics through a vortex core model and a modified surface boundary condition. The concept has been recently developed by the authors and shown to provide a better prediction capability for vortical flow field analysis.[13] The vortex core model has improved predictions of vortex breakdown and secondary vortices with little increase in computational cost. The modified surface boundary condition enhances the ability of Euler codes to predict the angle of attack at which a leading edge vortex appears on wings with round leading edges. The viscous models are derived from the Navier–Stokes equations and validated using simple test cases. Results for several highly swept wings are compared with those from experiments and from conventional Euler and Navier–Stokes solutions.

2. EULER ANALYSIS

The conventional premise is that a flow field can be modelled with the Euler equations if viscous effects do not alter the basic flow structure. The Euler equations bypass the computational issues associated with the small length scales in modelling viscous effects. However, flow field structures involving leading edge vortices are strongly influenced by air viscosity. Without proper viscous models a flow field analysis cannot accurately predict leading edge vortex separation, vortex core dynamics and vortex breakdown. In the present study, therefore, viscous effects are included by adding momentum source terms to the Euler equations.

The unsteady Euler equations are solved to obtain steady state solutions as time asymptotes. Including the momentum source terms for viscous effects, the time-dependent Euler equations can be written in vector form as

$$\frac{\partial W}{\partial t}+\nabla\cdot\mathbf{F}=S, \tag{1}$$

$$W=\begin{Bmatrix}\rho\\ \rho u\\ \rho v\\ \rho w\\ \rho E\end{Bmatrix},\qquad \mathbf{F}=\begin{Bmatrix}\rho\mathbf{q}\\ \rho u\mathbf{q}+p\hat{\mathbf{i}}\\ \rho v\mathbf{q}+p\hat{\mathbf{j}}\\ \rho w\mathbf{q}+p\hat{\mathbf{k}}\\ \rho E\mathbf{q}+p\mathbf{q}\end{Bmatrix},\qquad S=\begin{Bmatrix}0\\ \mathbf{Q}\cdot\hat{\mathbf{i}}\\ \mathbf{Q}\cdot\hat{\mathbf{j}}\\ \mathbf{Q}\cdot\hat{\mathbf{k}}\\ \mathbf{Q}\cdot\mathbf{q}\end{Bmatrix},$$

where ρ, p, E and $\mathbf{q}=(u, v, w)$ are the density, pressure, total energy and velocity vector of the flow. The right-hand side of equation (1) is the contribution of momentum sources representing the viscous effects. Instead of using the viscous stress terms of the Navier–Stokes equations, the

momentum source vector **Q** is explicitly defined using viscous models to be discussed in the following sections.

A surface-fitted co-ordinate system is adopted to facilitate the implementation of surface boundary conditions on configuration geometries. Equation (1) is then transformed into the generalized co-ordinate system and a finite volume method is used for the spatial discretization. All the flow variables are defined at cell centres. The use of a divergence-free form ensures the conservation of flow quantities. The centred difference scheme is adopted and flow-adaptive artificial viscosity terms are added for numerical stability. Integration in the time domain is performed explicitly using a fourth-order Runge–Kutta method. Since time accuracy is not sought, the time steps are defined locally to accelerate convergence.

Three different boundary conditions are implemented. Characteristic boundary conditions are imposed at the far-field boundary based on one-dimensional eigenvalue analysis. For planes of symmetry a mirror image condition is imposed for all the flow variables. The boundary condition on solid surfaces is the flow tangency condition. This solid wall boundary condition is incorporated with the viscous shear layer model to account for the momentum losses inside the shear layer. The pressure must be specified on solid wall boundaries and at the plane of symmetry. Conventionally in the Euler formulation the surface pressure is extrapolated from the infield points using the normal momentum equation. This extrapolation procedure is also modified in order to include viscous effects.

3. CORE MODEL DEVELOPMENT

A viscous model for the vortex core is derived from the steady, incompressible Navier–Stokes equations written for the cylindrical co-ordinate system centred on a vortex core. The vortex is assumed to be slender and close to a wing surface and a plane of symmetry. The vortex core diameter is assumed to be of the order of the square root of the Reynolds number. After eliminating the terms which become negligible for large Reynolds numbers and the terms involved in the circumferential direction, the non-dimensionalized equations of motion become

$$\frac{\partial(\rho u r)}{\partial x}+\frac{\partial(\rho v r)}{\partial r}=0, \tag{2a}$$

$$u\frac{\partial u}{\partial x}+v\frac{\partial u}{\partial r}=-\frac{1}{\rho}\frac{\partial p}{\partial x}+\frac{1}{Re\varepsilon^2}\left[\frac{1}{r}\frac{\partial}{\partial r}\left(r\frac{\partial u}{\partial r}\right)\right], \tag{2b}$$

$$\frac{w^2}{r}=\frac{1}{\rho}\frac{\partial p}{\partial r}, \tag{2c}$$

$$u\frac{\partial w}{\partial x}+v\frac{\partial w}{\partial r}+\frac{vw}{r}=\frac{1}{Re\varepsilon^2}\left[\frac{\partial}{\partial r}\left(\frac{1}{r}\frac{\partial}{\partial r}(rw)\right)\right]. \tag{2d}$$

Here the velocity components u, v and w are defined in the co-ordinates x, r and θ which correspond to the axial, radial and circumferential directions. In equation (2) the following non-dimensional parameters are defined:

$$\varepsilon\equiv\frac{\delta_{\text{ref}}}{L}, \qquad Re\equiv\frac{\rho U_\infty L}{\mu},$$

where L is the reference axial length scale of the vortex and δ_{ref} is the reference vortex core radius at $x=L$. The variables ρ and μ are the density and viscosity of the air respectively and U_∞ denotes

the freestream velocity. Length, velocity and pressure are normalized by L, U_∞ and ρU_∞^2 respectively. As in the boundary layer equations, the radial co-ordinate and its velocity component are scaled by the small parameter ε.

The above equations are integrated algebraically by defining axial and circumferential velocity profiles within the vortex core. Here the velocity profile implies the shape of the velocity distribution in the radial direction. The velocity profile defined by Mager[14] is adopted for the integration. Since Euler codes cannot accommodate a purely inviscid vortex which contains a singularity at the centre, the vortex model must have a rotational core as in the Rankine vortex. Also, there is a limitation on the vortex core size which can be resolved by Euler codes. Any core smaller than this limit will be diffused by numerical viscosity. Figure 1 shows the compatibility between Mager's model and results from a Euler code for profiles of circumferential velocity and circulation. Profiles for the Rankine vortex are also included for comparison. Note that the circulation around a vortex is constant outside the core.

Another consideration is the influence of the image vortex filaments associated with the wing surface boundary and the plane of symmetry (Figure 2). To include these effects, the Cartesian co-ordinate system is used, with X, Y and Z as streamwise, vertical and spanwise co-ordinates

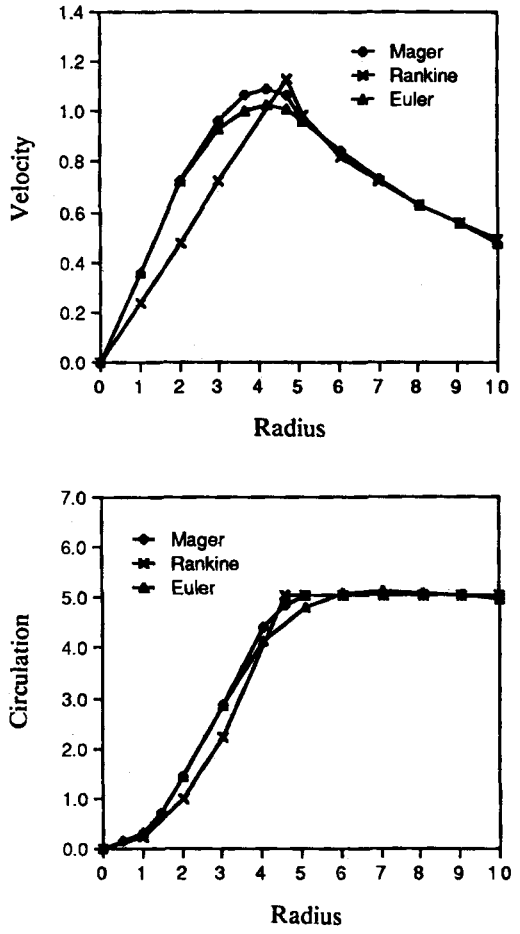

Figure 1. Vortex core structure

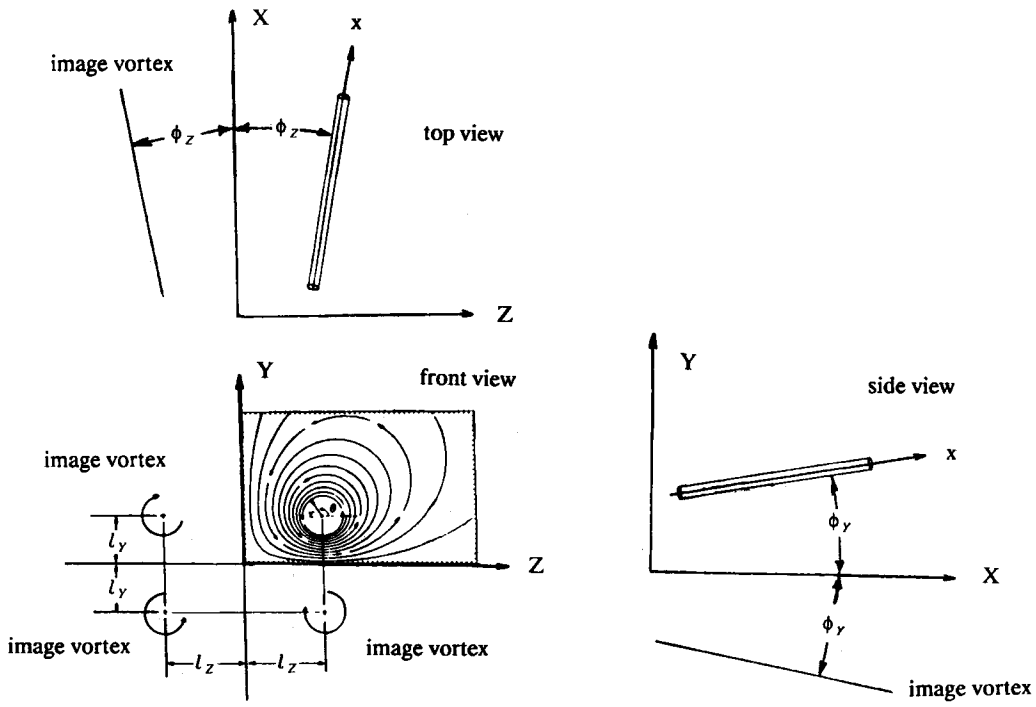

Figure 2. Vortex filament and its images

respectively. In this co-ordinate system two non-dimensional distances and two angles are defined as follows:

$$l_Y = \frac{Y_{\text{core}} - Y_{\text{wing}}}{\delta_{\text{ref}}}, \qquad l_Z = \frac{Z_{\text{core}} - Z_{\text{symm}}}{\delta_{\text{ref}}},$$

$$\phi_Y = \tan^{-1}\left(\frac{\mathrm{d}l_Y}{\mathrm{d}x}\right), \qquad \phi_Z = \tan^{-1}\left(\frac{\mathrm{d}l_Z}{\mathrm{d}x}\right).$$

First, with the specified circumferential velocity profile, equation (2c) is integrated from the core centre, $r=0$, to the edge of the core, $r=\delta$. Then the pressure at the vortex centre can be given by

$$p(x, 0) = p(x, \delta) - K_a \frac{\Gamma^2}{a} + K_i \Gamma^2 C_\phi. \tag{3}$$

The vortex core area a and the circulation Γ are defined as

$$a = \pi\delta^2, \qquad \Gamma = 2\pi\delta w_\delta,$$

where the subscript δ denotes the value at the core boundary. In equation (3) C_ϕ is the influence of the image vortices given by

$$C_\phi = \frac{\cos\phi_Y}{l_Y^2} + \frac{\cos\phi_Z}{l_Z^2} - \frac{\cos\phi_Y \cos\phi_Z}{l_Y^2 + l_Z^2}. \tag{4}$$

The coefficient K_a depends on the choice of the circumferential velocity profile and K_i accounts for the influence of image vortices.

It is assumed that the velocity profiles are similar in the axial direction, with the core diameter δ and the core edge axial velocity u_δ as the similarity parameters. Then the radial velocity profile can be obtained by integrating equation (2a) with respect to the radial direction. With profiles of the three velocity components known, equation (2d) is then integrated over the area of the vortex core to obtain

$$\frac{1}{a}\frac{da}{dx}=\frac{K_1}{\Gamma}\frac{d\Gamma}{dx}-\frac{K_2}{u_\delta}\frac{du_\delta}{dx}+\frac{K_3}{Re\varepsilon^2 a u_\delta}, \tag{5}$$

where the values of K_1, K_2 and K_3 depend on the velocity profiles chosen. For the Rankine vortex circumferential velocity profile K_2 and K_3 are zero and K_1 is one. In this case equation (5) implies that the vortex core area is a linear function of the vortex strength. For complex velocity profiles it is more difficult to integrate equation (5). If the last term is assumed to be independent of x, then the equation can be integrated to give

$$a=K_\theta\frac{\Gamma^{K_1}}{u_\delta^{K_2}}(x-x_0), \tag{6}$$

where K_θ is a core growth parameter which depends primarily on the product $Re\varepsilon^2$ and x_0 comes from the integration constant. Equation (6) serves as a model for the growth of the physical vortex core based on velocity profiles and parameters measured from the Euler solution.

Next, the circumferential velocity profile is assumed to be close to that of the Rankine vortex in order to approximate the radial distribution of pressure with

$$p(x, r)=p(x, 0)+\left(\frac{r}{\delta}\right)^2[p(x, \delta)-p(x, 0)]. \tag{7}$$

Using equations (3) and (7), equation (2b) is integrated over the area of the core to get the one-dimensional relation along the vortex core:

$$\left(\rho u\frac{du}{dx}+\frac{dp}{dx}\right)_0=-K_a\left(\frac{\Gamma}{a}\frac{d\Gamma}{dx}-\frac{\Gamma^2}{a^2}\frac{da}{dx}\right)+K_i\left(\Gamma\frac{d\Gamma}{dx}C_\phi-\frac{\Gamma^2}{2a}\frac{da}{dx}C_\phi+\frac{\Gamma^2}{2}\frac{dC_\phi}{dx}\right), \tag{8}$$

where the subscript 0 designates core centre values.

It is worthwhile to point out that the contribution of the viscous term disappears in the integration if the axial velocity profile is defined with zero slope at the centre and the edge of the core. Note that the coefficients K_a and K_i are functions of the velocity profiles and the location of the vortex core. If the velocity profiles of the viscous core and those in Euler solutions are similar, then the major discrepancy of the Euler formulation is primarily due to the non-physical estimation of the core size and the core growth rate. Therefore the non-physical vortex core in Euler solutions can be replaced with a core that is derived from viscous physics, as given in equation (8). This is in effect equivalent to an addition of the difference between the model and the Euler solution as a source term into the Euler formulation. The difference can be given as

$$\left(\rho u\frac{du}{dx}+\frac{dp}{dx}\right)_0-\left(\rho u\frac{du}{dx}+\frac{dp}{dx}\right)_{0_E}=-K_a\left[\frac{\Gamma}{a}\frac{d\Gamma}{dx}\left(1-\frac{a}{a_E}\right)-\frac{\Gamma^2}{a^2}\left(\frac{da}{dx}-\frac{a^2}{a_E^2}\frac{da_E}{dx}\right)\right]$$
$$-K_i\frac{\Gamma^2}{2a}C_\phi\left(\frac{da}{dx}-\frac{a}{a_E}\frac{da_E}{dx}\right), \tag{9}$$

where the subscript E denotes flow quantities measured in the Euler solution. Similarly, the correction to pressure at the core centre is given by

$$p(x,0)-p(x,0)_E=-K_a\frac{\Gamma^2}{a}\left[1-\left(\frac{a}{a_E}\right)^2\right]+K_i\Gamma^2\left(1-\frac{a}{a_E}\right)C_\phi. \tag{10}$$

Equation (9) provides the momentum source terms for use in the right-hand side of the Euler equations, as shown in equation (1). Again the control parameters K_θ, K_a and K_i depend primarily on the velocity profiles of the physical vortex. Equation (10) represents a correction to the vortex core pressure in the Euler solution based on the ratio of the size of the model core to the size of the core in the Euler solution.

4. SHEAR LAYER MODELLING

Vortex roll-up is initiated by boundary layer separation near the leading edges of highly swept wings. Without viscous models for the shear layer of the three-dimensional separation, Euler solvers create leading edge separation by numerical diffusion, which is again a function of grid quality, grid size and the numerical algorithm. Also, the downstream vortex strength depends on the location where the separation begins, which cannot be determined *a priori* for wings with round leading edges.

The momentum equations for the control volume next to the wing surface require knowledge of the pressure on the wing surface. Two different methods for estimating the pressure on the wing surface were tested. The first method uses the normal momentum equation from the Euler formulation to extrapolate pressure from the cell centre down to the wing surface. When this method is used, the appearance of leading edge vortices in the flow solution was delayed to higher angles of attack than those obtained from wind tunnel tests. The second method equates the pressure at the wing surface to the pressure at the centre of the boundary cell by assuming zero normal pressure gradient as in the boundary layer. When this boundary condition is used, the vortices start to appear at lower angles of attack. This effect of the surface pressure boundary condition on the appearance of the leading edge vortex separation is shown in Figure 3.

The flow phenomena inside the viscous shear layer near the wing are too complex to model with simple physics. The flow field involves many different features, including the mechanism for

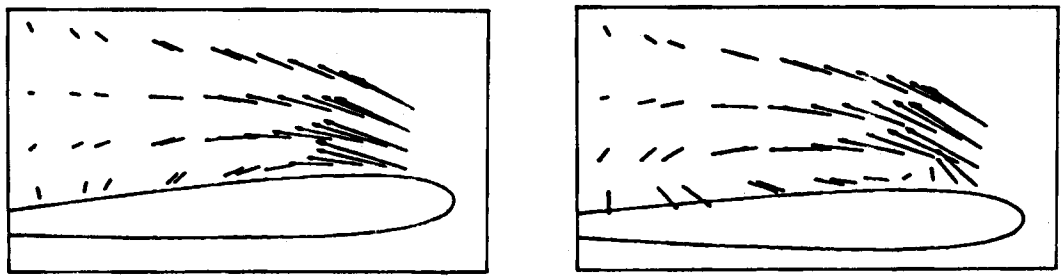

Figure 3. Effect of surface pressure boundary condition on appearance of leading edge vortex separation—cross-flow velocity vectors for an arrow wing at $\alpha=18°$: (a) surface pressure extrapolated using the normal momentum equation; (b) surface pressure extrapolated by assuming zero normal pressure gradient

creating leading edge vortices, reattachment of the primary vortex, appearance of a secondary vortex separation, etc. Instead of attempting to model these complex phenomena, the influence of the shear layer on the vortex system is included through a simple model. Two major characteristics, shear layer thickness and wall shear stress, are identified and modelled with formulae borrowed from the incompressible turbulent boundary layer on a flat plate. That is, the wall shear layer thickness and the skin friction coefficient are defined from

$$\delta_{\text{wall}} = \frac{K_\delta l}{(Re_{\text{local}})^{0.2}}, \tag{11}$$

$$C_f = \frac{K_\tau}{(Re_{\text{local}})^{0.2}}, \tag{12}$$

where Re_{local} is the local Reynolds number based on the distance l measured from the apex of a delta wing. The coefficients K_δ and K_τ are input specified constants with values of 0·37 and 0·074 respectively for the flat plate. The shear stress effect is added into the momentum equations in the direction of the surface velocity vector as source terms. The shear layer thickness effect is accounted for in the surface pressure estimation by using

$$p_{\text{wall}} = p_{\text{cell}} - \frac{dp}{dn}(\Delta - \delta_{\text{wall}}), \tag{13}$$

where p_{cell} is the pressure at the neighbouring boundary cell, dp/dn is the pressure gradient in the normal direction and Δ is the normal distance between the two points. If δ_{wall} is set to zero, the equation implies that the wall pressure is obtained through a purely inviscid calculation.

5. MODEL IMPLEMENTATION

The vortex core model is implemented in the Euler solver as a separate subroutine and accessed periodically. The total circulation or vortex strength and the Euler vortex core size are measured from Euler solutions at each axial location along the vortex. The vortex strength is obtained by evaluating the vorticity fluxes through the surfaces of each cell and summing them. The area of the vortex core is measured from the cross-sectional areas of the cells which contain vorticity of strength above a given threshold level. The centre of the vortex at each axial station is identified as the cell with a local minimum static pressure and a local maximum vorticity flux. Locating the vortex centre establishes the values of C_ϕ in equation (4).

The momentum source term in the vortex core direction and the correction to the pressure at the vortex centre are obtained from equations (9) and (10). These quantities are added to the flow solver for subsequent iterations. To avoid destabilizing the solution process, the momentum source terms are not just applied to the cell at the vortex centre. The source terms for the neighbouring cells are scaled in accordance with their distance from the centre following a profile similar to the axial velocity profiles used by Mager. In order to reduce computational costs, these corrections are updated every 30 iterations.

The viscous layer model for the surface boundary condition is also incorporated into the Euler solver. The pressure at the surface is defined using equation (13) to include the viscous layer thickness effect. The shear stress in equation (12) defines source terms for the boundary cells. The source terms are added to the Euler equations in the direction parallel to the surface velocity vector. As in the vortex core model, the corrections for the surface boundary condition model are updated periodically.

6. RESULTS

The vortex core model was first examined with a simple vortex filament introduced in the direction of the freestream near a solid wall and a plane of symmetry.[13] The numerical viscosity included in inviscid Euler calculations produces a finite vortex core. Refined grids reduce the core size. Axially expanding grids enlarge the vortex core downstream. The enlarged core reduces the circumferential velocity component and hence increases the core pressure. The grid-induced adverse pressure gradient along a vortex core may cause a reversal in the axial velocity component inside the core, as in vortex bursting. The developed vortex core model can eliminate the grid-induced axial velocity defect by linking the core pressure to the physical core size instead of the grid-dependent core size. On the other hand, if a sufficient rate of growth of the physical core is assumed, the model produces an axial flow reversal on a uniform grid. This implies that, unlike the Euler solver alone, the Euler code with model can produce a flow reversal depending on physical parameter values instead of relying on numerics.

The ability of the developed core model to predict the onset of bursting was assessed on four different flat plate delta wings, three with sweep angles of 55°, 65° and 75° and the other with an aspect ratio of 1·0. All the calculations were performed at a Mach number of 0·2 and a Reynolds number of 10^6. Figure 4 shows a typical H-O grid topology used for these tests. Figure 5 shows

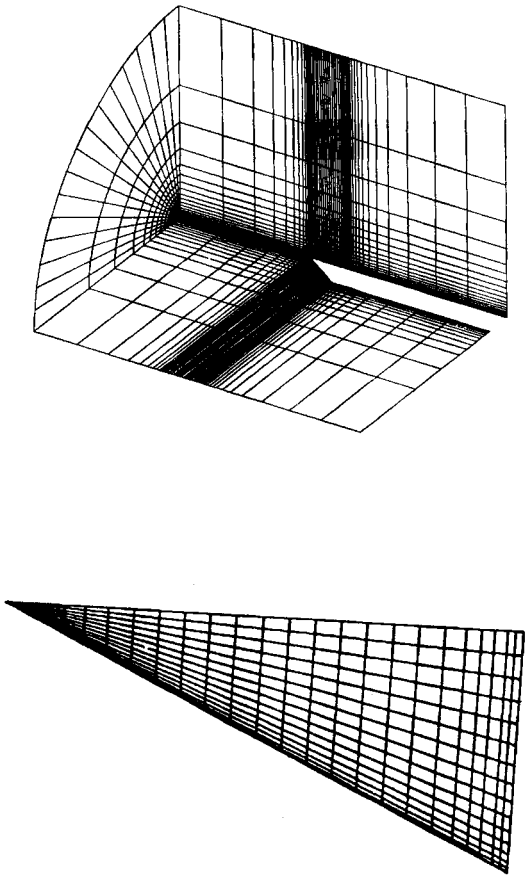

Figure 4. Grid topology to study vortex bursting on delta wings

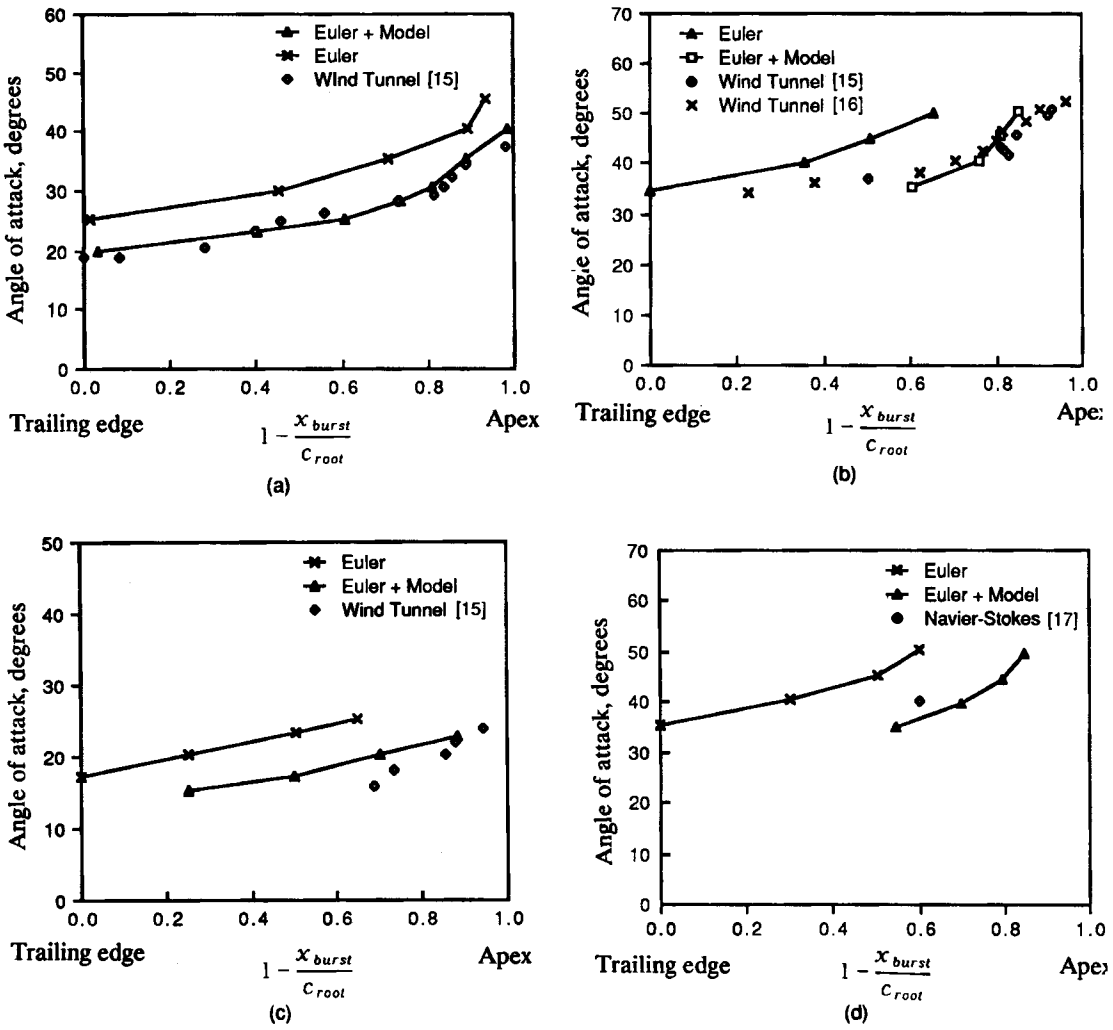

Figure 5. Predictions of vortex-bursting locations: (a) 65° delta wing; (b) 75° delta wing; (c) 55° delta wing; (d) aspect ratio 1·0 delta wing

bursting location versus angle of attack curves from the Euler solver with the vortex core model compared with results from wind tunnels,[15,16] Euler solvers alone and Navier–Stokes solvers.[17] In all these tests the parameters K_θ, K_a and K_i were held constant. No special treatment was given on the vortex core model downstream of the vortex burst. Although the core model is not valid downstream of the bursting point, the same core model was used with a large core size. For each wing tested, the Euler code and core model were able to produce results in closer agreement with wind tunnel tests and Navier–Stokes codes than did the Euler solver alone. Figure 6(a) compares velocity vectors in the horizontal plane containing the vortex for an aspect ratio 1·0 delta wing at 40° angle of attack. The result from the Euler code alone shows the bursting point at an axial station about 70% root chord downstream of the wing apex. The Euler code and model give the bursting point at about 30% root chord, which agrees better with Navier–Stokes results.

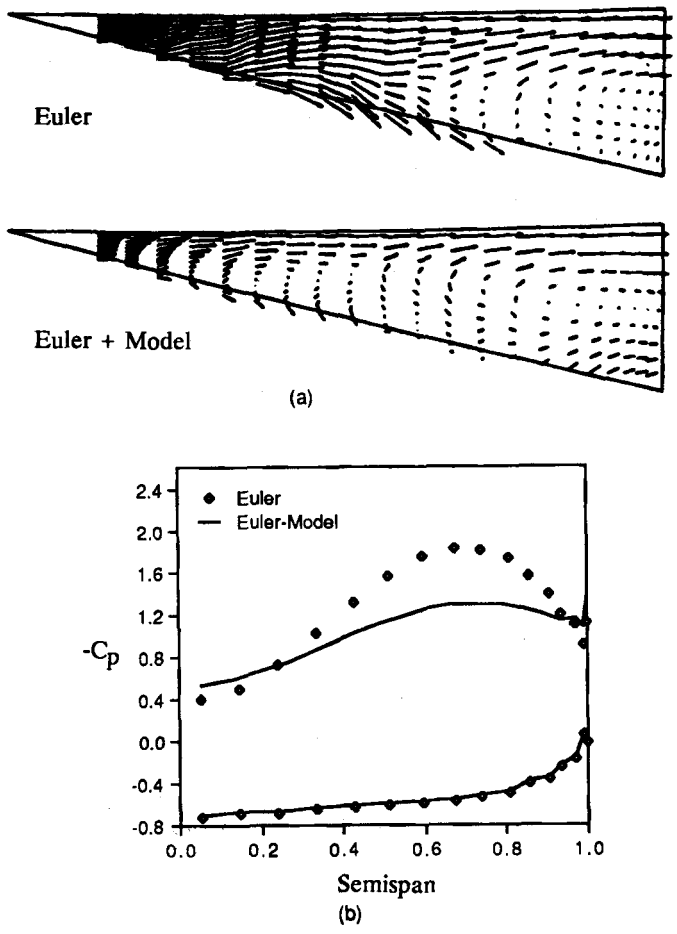

Figure 6. Effect of vortex core model for aspect ratio 1·0 delta wing at $\alpha = 40°$: (a) velocity vectors on a horizontal plane near the vortex core; (b) surface pressure at 50% root chord

Figure 6(b) compares the corresponding C_p-curves for the two solutions at 50% root chord. The vortex at that station has burst in the solution using the model but not in the conventional Euler solution. Note the flattening of the C_p-curve when bursting has occurred.

The surface boundary condition with the viscous layer model was tested on an arrow wing. This test was carried out at a Mach number of 0·4 and a Reynolds number of 2×10^6. Figure 7 shows the typical C-mesh topology used for this study. Figure 8 illustrates the effect on surface pressure distribution of changing K_δ of the shear layer model while holding the Reynolds number equal to that of the wind tunnel test.[18] A value of 2·1 for K_δ appears to give the best result. Figure 9 compares surface pressure contours from wind tunnel tests with those from a Euler solver using the viscous layer model surface boundary condition for a range of angles of attack, exhibiting consistent agreement.

Also considered is the simple shear stress model which accounts for the effects of velocity defects in the viscous layer through momentum source terms in the boundary cells. Figure 10 compares two cross-flow velocity vector plots for a 65° swept delta wing with round leading edges. A Mach number of 0·2 and a Reynolds number of $0{\cdot}9 \times 10^6$ were used in these calculations.

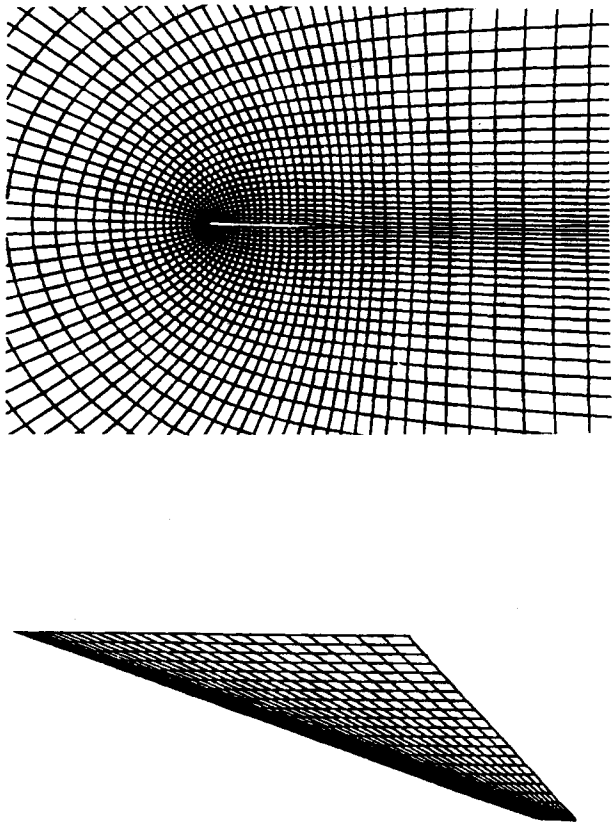

Figure 7. C-mesh topology used with shear layer model

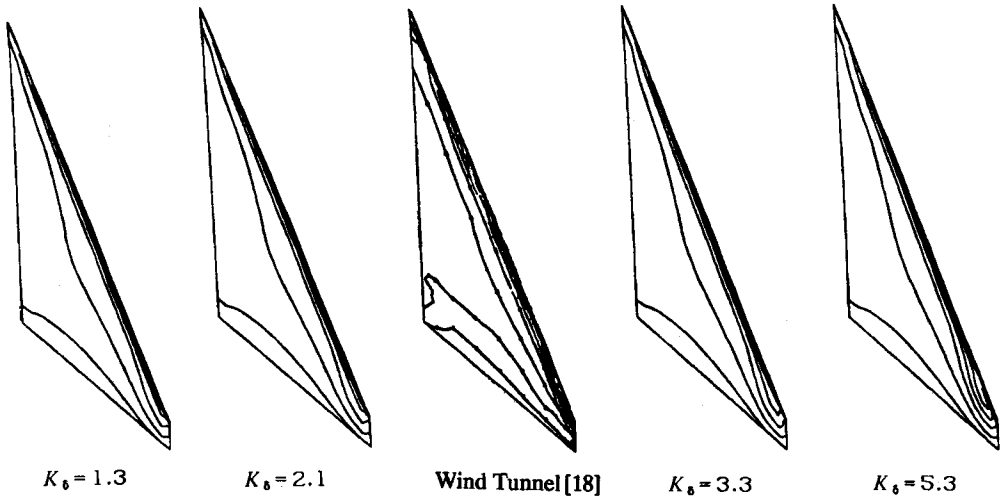

Figure 8. Effect of shear layer growth parameter—surface pressure contours for an arrow wing with round leading edges at $\alpha = 4°$

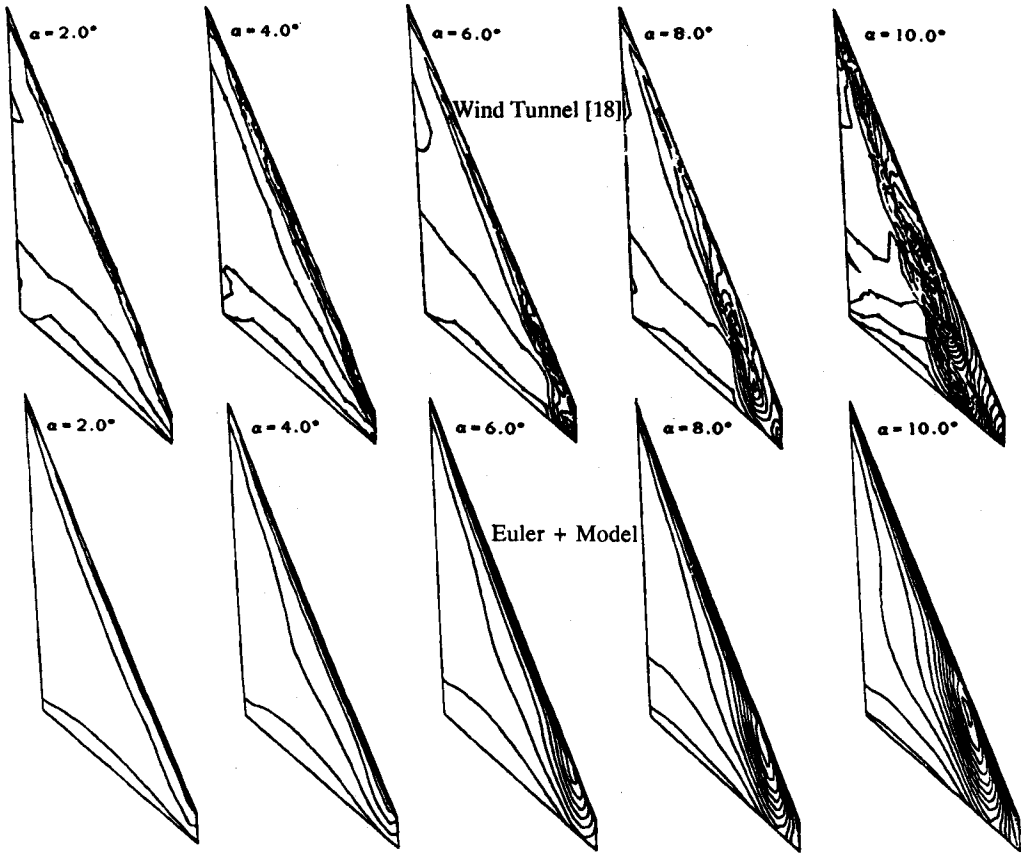

Figure 9. Comparison of surface pressure contours with wind tunnel tests at various angles of attack

Figures 11 and 12 also compare the surface pressures and the surface velocity vectors respectively, showing that the shear layer model can capture the appearance of the secondary vortex near the wing tip. The location and strength of this secondary vortex are in qualitative agreement with results from Navier–Stokes solutions[17] and wind tunnels.[19] Because such secondary vortices are not normally seen in Euler solutions,[2,3] these preliminary results are encouraging, although further refinement of the viscous layer model is required.

7. CONCLUSIONS

A computational approach has been developed which incorporates viscous models from the Navier–Stokes physics into Euler solvers. The inviscid/viscous coupling provides corrections to the inviscid Euler formulation in the form of momentum source terms. The combination of Euler code and core model has been shown to give predictions of vortex-bursting points on delta wings which are in better agreement with wind tunnel tests and Navier–Stokes solutions than can be achieved by a Euler code alone. Surface pressure predictions are also improved. The model reduces the effects of grid stretching and artificial viscosity which may cause numerical vortex

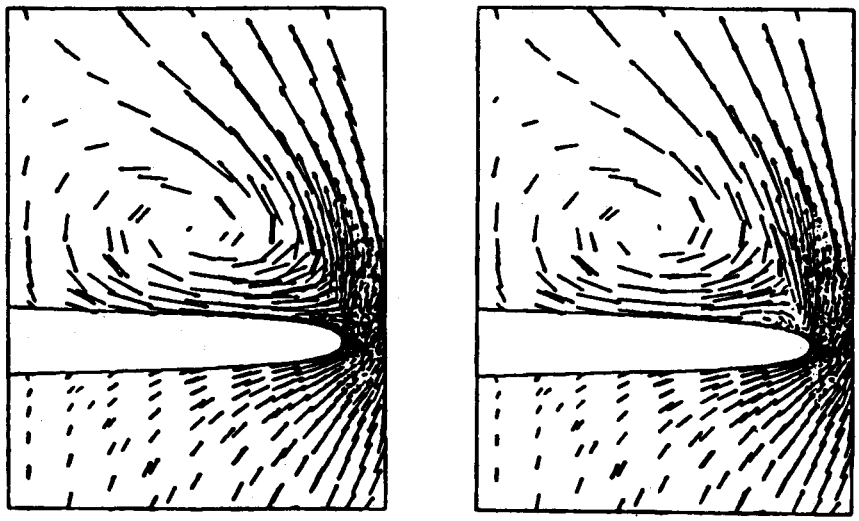

Figure 10. Effect of shear layer model—cross-flow velocity vectors at 50% root chord of a 65° delta wing with round leading edges at $\alpha = 40°$

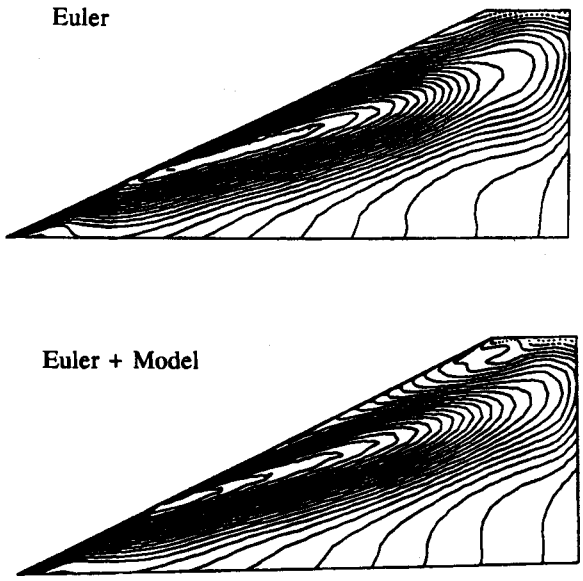

Figure 11. Effect of shear layer model—surface pressure contours on a 65° delta wing with round leading edges at $\alpha = 20°$

bursting in Euler solutions and captures physical vortex bursting as in Navier–Stokes solutions. These capabilities are achieved at a very modest cost.

A simple model was also used to include the viscous physics of the wall shear layer through the surface boundary condition in Euler solvers. An approximation of the total pressure loss in the viscous layer near the wing surface provides a boundary condition which is closer to the actual

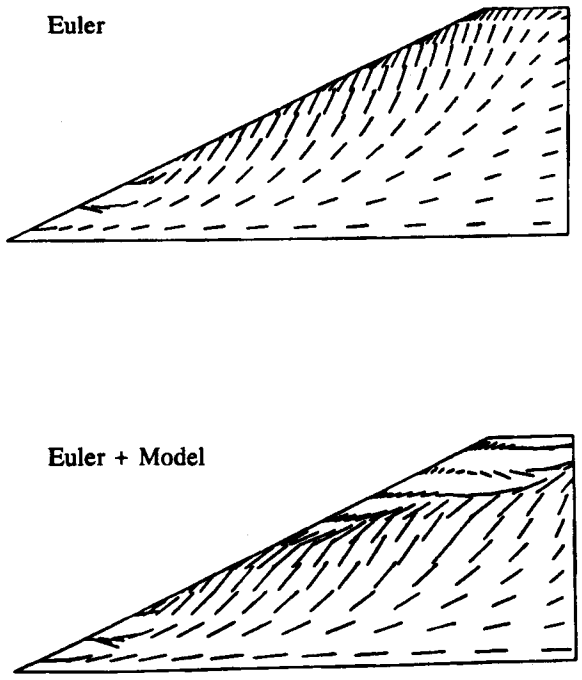

Figure 12. Effect of shear layer model—surface velocity vectors on a 65° delta wing with round leading edges at $\alpha = 20°$

physics. Prediction of leading edge separation and vortex roll-up on highly swept wings with rounded leading edges is improved. The use of a more refined model for the viscous layer would further enhance the performance of the method. It has also been demonstrated that inclusion of momentum defects near the wing surface can lead to the appearance of secondary vortices in Euler solutions.

The major merit of the presented approach is the ability to produce improved predictions for vortex-dominated flows consistently and at comparatively low cost. Although successful results have been demonstrated, further refinement and fine tuning of the viscous models are needed.

ACKNOWLEDGEMENTS

The authors wish to thank James Loellbach and Moon-Sang Kim for their assistance in preparing this paper. Advice and encouragement from Dr. Raymond Cosner and Dr. August Verhoff of McDonnell-Douglas are also gratefully acknowledged.

REFERENCES

1. E. M. Murman and A. Rizzi, 'Applications of Euler equations to sharp edge delta wings with leading edge vortices', *Application of Computational Fluid Dynamics in Aeronautics*, AGARD-CP-412, AGARD, Loughton, 1986, pp. 15: 1–13.
2. A. Rizzi, G. Drougge and C. J. Purcell, 'Euler simulation of shed vortex flows over the 65 degree delta wings', *Proc. Symp. on International Vortex Flow Experiment on Euler Code Validation*, 1986, FFA, Bromma, Sweden 1986, pp. 289–343.
3. J. R. Sirbaugh, 'Euler analysis of the AFWAL 65 degree delta wing', *Proc. Symp. on International Vortex Flow Experiment on Euler Code Validation*, 1986, FFA, Bromma, Sweden 1986, pp. 245–268.

4. R. W. Newsome and J. L. Thomas, 'Computation of leading edge vortex flows', *Vortex Flow Aerodynamics, Vol. 1, NASA CP 2416*, 1985, pp. 305–330.
5. D. P. Rizzetta and J. S. Shang, 'Numerical simulation of leading-edge vortex flows', *AIAA J.*, **24**, 237–245 (1986).
6. O. A. Kandil, A. H. Chuang and J. M. Shifflette, 'Finite-volume Euler and Navier–Stokes solvers for three-dimensional and conical vortex flows over delta wings', *AIAA Paper 87-0041*, 1987.
7. H. W. M. Hoeijmakers, 'Methods for numerical simulation of leading edge vortex flow', *Studies of Vortex Dominated Flows*, Springer, New York, 1987, pp. 223–269.
8. R. W. Newsome and O. A. Kandi, 'Vortical flow aerodynamics—physical aspects and numerical simulation', *AIAA Paper 87-0205*, 1987.
9. K. Fujii and L. B. Schiff, 'Numerical simulation of vortical flows over a strake-delta wing', *AIAA Paper 87-1229*, 1987.
10. C. H. Hsu and C. H. Liu, 'Navier–Stokes computation of flow around a round-edged double-delta wing', *AIAA Paper 88-2560-CP*, 1988.
11. P. Raj and L. N. Long, 'An Euler aerodynamic method for leading-edge vortex flow simulation', *Vortex Flow Aerodynamics, Vol. 1, NASA CP 2416*, 1985, pp. 263–281.
12. S. M. Hitzel, 'Wing vortex-flows up into vortex-breakdown—a numerical simulation', *AIAA Paper 88-2518-CP*, 1988.
13. K. D. Lee and S. A. Brandt, 'Modeling of vortex dominated flowfields in the Euler formulation', *ICAS-88-5.9.3, 16th ICAS Proc.*, Jerusalem, 1988, AIAA, Washington, D.C., 1988, pp. 1437–1450.
14. A. Mager, 'Dissipation and breakdown of a wingtip vortex', *J. Fluid Mech.*, **55**, 609–628 (1972).
15. W. H. Wentz and D. L. Kohlman, 'Vortex breakdown on slender sharp-edged wings', *J. Aircraft*, **8**, 156–161 (1971).
16. F. M. Payne and R. C. Nelson, 'An experimental investigation of vortex breakdown on a delta wing', *Vortex Flow Aerodynamics. Vol. 1, NASA CP 2416*, 1985, pp. 135–161.
17. P. M. Hartwich, C. H. Hsu, J. M. Luckring and C. H. Liu, 'Numerical study of the vortex burst phenomenon for delta wings', *AIAA Paper 88-0505*, 1988.
18. M. E. Manroe, K. J. R. Manning, T. H. Halstaff and J. T. Rogers, 'Transonic pressure measurements and comparison of theory to experiment for an arrow-wing configuration', *NASA CR 2610*, August 1976.
19. D. Hummel, 'On the vortex formation over a slender delta wing at large angles of incidence', *AGARD-CP-247*, 1978, Paper 15.